Peer-reviewed version available at Minerals 2018, 8, 221; doi:10.3390/min8060221

Article

Quick, Easy and Economic Mineralogical Studies of Flooded Chalk for EOR Experiments Using Raman Spectroscopy

Laura Borromeo[1, 2, *], Nina Egeland[1, 2], Mona Wetrhus Minde[1, 2], Udo Zimmermann[1, 2], Sergio Andò[3], Merete Vadla Madland[1, 2], Reidar Inge Korsnes[1, 2]

[1] Department of Energy Resources, University of Stavanger, Norway
[2] The National IOR Centre of Norway, Stavanger, Norway
[3] Department of Earth and Environmental Sciences, University of Milano - Bicocca, Milano, Italy
* Correspondence: laura.borromeo@uis.no; Tel.: +39 3386008504

Abstract: Understanding the chalk-fluid interactions and the associated mineralogical and mechanical alteration at sub-micron scale are major goals in Enhanced Oil Recovery. Mechanical strength, porosity, and permeability of chalk are linked to mineral dissolution that occurs during brine injections, and affect the reservoir potential. This paper presents a novel „single grain" methodology to recognize the varieties of carbonates in rocks and loose sediments: Raman spectroscopy is a non-destructive, quick, and user-friendly technique representing a powerful tool to identify minerals down to 1 µm. An innovative working technique for oil exploration is proposed, as the mineralogy of micron-sized crystals grown in two flooded chalk samples (Liége, Belgium) was successfully investigated by Raman spectroscopy. The drilled chalk cores were flooded with $MgCl_2$ for c. 1.5 (Long Term Test) and 3 years (Ultra Long Term Test) under North Sea reservoir conditions (Long Term Test: 130°C, 1 PV/day, 9.3 MPa effective stress; Ultra Long Term Test: 130°C, varying between 1-3 PV/day, 10.4 MPa effective stress). Raman spectroscopy was able to identify the presence of recrystallized magnesite along the core of the Long Term Test up to 4 cm from the injection surface, down to the crystal size of 1-2 µm. In the Ultra Long Term Test core the growth of $MgCO_3$ affected nearly the entire core (7 cm). In both samples, no dolomite or high-magnesium calcite secondary growth could be detected when analysing 557 and 90 Raman spectra on the Long and Ultra Long Term Test, respectively. This study can offer Raman spectroscopy as a breakthrough tool in petroleum exploration of unconventional reservoirs, due to its quickness, spatial resolution, and non-destructive acquisition of data. These characteristics would encourage its use coupled with electron microscopes and energy dispersive systems or even electron microprobe studies.

Keywords: flooded chalk; Raman spectroscopy; Enhanced Oil Recovery; carbonates; calcite; magnesite.

1. Introduction

Injection of seawater-like brines is one of the most successful Improved Oil Recovery (IOR) methods on the Norwegian Continental Shelf [amongst many others: 1,2]. The mechanical strength of chalk is weakened by seawater at reservoir temperatures, and as a consequence, compaction and loss in porosity occur, affecting the oil recovery factor of carbonate fields [3-10]. It is important to understand how fluids interact with rocks because textural and chemical/mineralogical changes in the pore space affect the way water will adsorb and expel oil from the rock [3, 8, 11-17]. Previous research on fluid injection has been carried out [5, 8, 17-21] and three ions have proven to play important roles when chalk is exposed to seawater at elevated temperatures: Ca^{2+}, Mg^{2+}, and SO_4^{2-}. The injected seawater triggers several mechanisms such as precipitation, dissolution, ion exchange, adsorption, and desorption, to interplay at the same time, with different relative significance depending on the position in the reservoir (nearby to the injector or to the producer). It is therefore

beneficial to simplify the system and study each ion individually. With $MgCl_2$ brines, which represent simplified aqueous chemistry of seawater, the role of Mg^{2+} is specifically studied.

The two cores investigated in this study (see Fig. 1), were flooded with $MgCl_2$ for 1.5 (Long Term Test, LTT) and 3 years (Ultra Long Term Test, ULTT) under reservoir conditions (LTT: 130°C, 1 PV/day, 9.3 MPa effective stress, ULTT: 130°C, varying between 1-3 PV/day, 10.4 MPa effective stress), in order to reach a mineralogical insight of the basic processes that happen during long time brine injection.

The analyses are carried out by Raman spectroscopy, which is a quick and versatile information-rich technique that can easily be applied to almost all substances (gases, liquids, solids, organic, and inorganic) with the only exception of metals. In the last decades Raman spectroscopy has proven to be an easy way to obtain mineral identification (see Fig. 2) [22-27] as every Raman spectrum is like a fingerprint that can provide various information such as crystallinity, phase, intrinsic stress/strain, and polymorphism [28-31]. Furthermore, mineral phases can be identified down to a few microns [32], a possibility of paramount importance in chalk investigation. By applying Raman to flooded chalk, a „grain by grain“ methodology was developed to obtain a better understanding of its mineralogy.

2. Materials and Methods

2.1. Samples

The samples studied in this project are all chalk, fine-grained carbonate rocks, built primarily of the skeletal debris of micro- and nano-organisms, mainly coccoliths, shed from coccolithophores (see SEM images in Fig. 3). The cores were sampled at the Lixhe outcrop (Gulpen Formation, Campanian to late early Maastrichtian) [33] near Liège in Belgium, in particular from the Zeven Wegen Member [34] with an age of 75.5–78.0 Ma. The chalk shows clear signs of recrystallization, contact cements, and particle interlocking. Nevertheless, coccoliths are still well preserved and the rock presents intrafossil porosity [35]. The chalk from Liège shows a clean compositional nature, as the main mineral component is calcite ($CaCO_3$) together with minor abundances of non-carbonate material (between 3-5 wt.% in total) [36, 37] that mainly consists of quartz, smectite/mixed smectite-illite layer, mica, kaolinite, and clinoptilolite, and minor amounts of zeolite, apatite, opal, feldspar, pyroxene, pyrites, and titanium oxide [36, 38].

The porosities lie in the range of 40-45 % [21, 35, 39-42]. More information about mineralogy, petrography, and rheological characteristics of these chalk successions can be found in literature [35, 39, 40-42]. Onshore chalk successions are used as analogues for North Sea reservoir chalk in several studies [8, 17, 20, 21, 35].

2.2. Flooding experiments

For this study, two long-term tests were analysed. Both cores were flooded with $MgCl_2$ at reservoir conditions. The chalk cores (length: ~70 mm, diameter: ~38 mm) were mounted into triaxial cells that allow for measurements of axial strains while flooding of reactive fluids at elevated pressures, stresses, and temperatures. Each triaxial cell was equipped with a heating jacket and a regulation system that kept the temperature constant at 130 ± 0.1°C throughout the experiment. To avoid boiling at temperatures above 100°C, a pore pressure of 0.7 MPa was applied prior to the heating of the system. While distilled water was injected to ensure a clean pore system and to clean the sample, the confining pressure and pore pressure were simultaneously increased from 0.5 and 0 MPa to 1.2 and 0.7 MPa, respectively, with a constant effective stress equal to 0.5 MPa Then, the hydrostatic pressure was increased to 10.0 MPa (LTT) and 11.1 MPa (ULTT). A 0.219 M $MgCl_2$ brine was injected with a flooding rate of 1 pore volume per day (PV/day) for the LTT and varying between 1-3 PV/day for the ULTT. The effective stress was 9.3 MPa and 10.4 MPa for the LTT and the ULTT, respectively. After the experiment was finished, the cores were cleaned, and after drying, cut into slices with thicknesses of about 10 mm (LTT; to the left in Fig. 1) and of about 35 mm (ULTT; to the right in Fig. 1); the samples were then investigated with different methods. For detailed information

Peer-reviewed version available at Minerals 2018, 8, 221; doi:10.3390/min8060221

of the performed tests, the reader is referred to Zimmermann et al. (2015) [36] for the LTT and Nermoen et al. (2015) [43] for the ULTT.

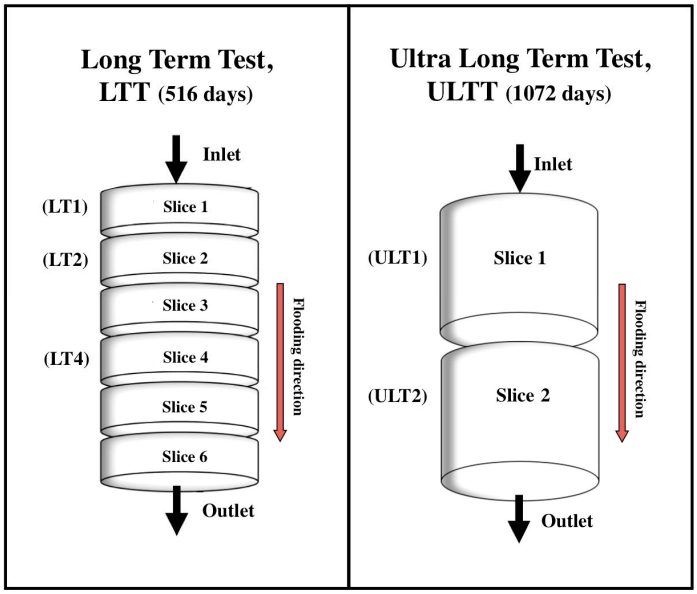

Figure 1. Schematic drawings of how the two cores were cut after the flooding experiment: Long Term Test (LTT) to the left (modified from Zimmermann et al. 2015 [36]) and Ultra Long Term Test to the right.

2.3. Field Emission Gun-Scanning Electron Microscopy with Energy-Dispersive Spectroscopy

Field Emission Gun-Scanning Electron Microscopy with Energy-Dispersive Spectroscopy (FEG-SEM) analyses were performed at the University of Stavanger using a Zeiss Supra VP 35. Freshly chipped off pieces of slices from the three core samples were analysed together with chips of unflooded chalk from the end-pieces of the same cores. The samples were coated with palladium ensuring a steady flux of electrons. The microscope parameters were set at an acceleration voltage between 12 to 15kV, 30 μm aperture, and a working distance between 10 and 12 mm. The high current setting was used. To perform qualitative and semi-quantitative analyses of the chemical composition of the imaged areas an EDAX energy-dispersive x-ray spectroscopy (EDS) system was used. To optimize the quantification results, and because the chalk predominantly consists of calcite, an Iceland spar calcite crystal was used to calibrate the system [36].

2.4. Raman spectroscopy

During this study, most of the spectra (465 of 557; reported with "**H**" in figures and Table 1) were collected with a Horiba XploRA Raman spectrometer equipped with an Olympus microscope with maximum magnification of 100x, and a motorized x–y stage. Calibration of spectra was obtained using a silicon wafer with a main peak at 520.7 cm^{-1} as reference and maintained during the analysis with a constant checking of the position of a sharp neon lamp emission line at 476.8 cm^{-1}. Other spectra (92 of 557; LTT slice 1: p1_G and I; p2_D and E; slice 4: C and D; reported with "**R**" in Fig. 2) were obtained using a high-resolution Renishaw inVia Reflex confocal Raman microscope, equipped with a Leica DM2500 polarizing microscope (maximum magnification of 100x) and motorized x–y stages. With both spectrometers, spectra were collected with a 532 nm line, solid-state lasers (10 mW at the sample), laser spot around 1 μm, spectral resolution of ±1 cm^{-1}, acquisition time of 1-2 minutes, magnification of 100x. Microscope pictures were taken for each beamed grain or cluster of grains. The spectral region found to be the most important and convenient to our study was the low-medium one; setting the XploRA spectrometer with a 2400 lines/mm grating in back-scattering configuration allowed us to collect in the spectral range 100-1200 cm^{-1}. Using a grating of 1800 lines/mm with the

inVia spectrometer instead, allowed us to collect in the range of 140-1900 cm^{-1}. In order to try to detect the occurrence of hydrated silicates, the region between 2900 and 4200 cm^{-1} was investigated collecting 200 spectra with the Renishaw inVia Reflex confocal Raman microscope at 100x of magnification.

Determination of the position of the peaks was performed through the Gaussian - Lorentzian (Pseudo Voight) deconvolution method, with an accuracy of 0.2 cm^{-1}, using the software *Labspec 5*, utilized also for baseline subtraction that helped to eliminate the occasional fluorescence of carbonates. Fluorescence and Raman scattering have similar origins, as both involve the inelastic scattering of photons. Practically, fluorescence represents a strong background noise that can obliterate the Raman signal. To avoid this phenomenon, chalk cores were not analysed directly on the rock surface but as very small amounts of powder that were scraped off with a needle from the rock, placed and spread on a glass slide. As the quantity required is almost negligible, and no specific preparation is needed to perform these analyses, Raman procedure allows for further investigation with other instrumentation if needed.

2.5. Raman spectroscopy on carbonates

For their large diffusion and good Raman signal, carbonates have been investigated in detail, with particular attention to thermodynamic properties and their vibrational spectra (23, 25, 44-49). Their Raman peaks positions are influenced by the magnesium content and crystallographic structure and allow in distinguishing calcite from Mg-calcite, aragonite, magnesite, huntite, and dolomite [32, 45, 49-52]. Carbonate minerals show comparable spectra as their structure is quite similar; a consistent increase in Raman shifts according to their Mg content occurs between calcite and magnesite, as a consequence of increased inter-atomic distances following the substitution of Ca^{2+} with the smaller Mg^{2+} ion in the cell [23, 45, 53]. This shift assists in distinguishing between the different carbonates.

Carbonate group minerals spectra (see Fig. 2) present four main peaks which can be divided into internal vibrations of the $(CO_3)^{2-}$ group (symmetric stretching, 600 – 1200 cm^{-1}, and asymmetric stretching, 1200 – 1700 cm^{-1}) [38, 45, 52, 54-56] and into lattice vibrations involving translation and librations of the $(CO_3)^{2-}$ group relative to the Ca^{2+} or Mg^{2+} ions (100 – 500 cm^{-1}). The strongest and sharpest peak (ν_1, *symmetric stretching mode* of the carbonate ion) is present around 1086 – 1095 cm^{-1} (calcite – magnesite respectively) along with other subsidiary bands at 150 – 215 cm^{-1} (T, *translational mode*), 280 – 330 cm^{-1} (L, *librational mode*), and 712 – 738 cm^{-1} (ν_4, *in-plane bending* of the $(CO_3)^{2-}$ group) [45, 57, 58].

2.6. Earlier studies and characterisation of the sample material

Various high-resolution methods were used to study mineralogical alteration in flooded chalk: field emission gun scanning electron microscopy– energy-dispersive X-ray spectroscopy (FEG-SEM-EDS) [3, 5, 8, 14, 36, 38, 59], nano secondary ion mass spectrometry (NanoSIMS) [36, 50, 60], x-ray diffraction (XRD) [36], whole-rock geochemistry techniques [36, 37, 60], Tip-Enhanced Raman Spectroscopy-Atomic Force Microscopy (TERS-AFM) [61, 62], Transmission Electron Microscopy (TEM) [59, 63], Mineral Liberation Analysis (MLA) [59]. The authors (LTT [36], and ULTT [43]) determined a loss of Ca^{2+} and a gain in Mg^{2+}, demonstrating a precipitation of new Mg-minerals in the core. FEG-SEM and TEM images have shown magnesite crystals with a grain size between 100 nm and 1 μm [59, 63].

Based on geochemical methods, Zimmermann et al. (2015) [36] could calculate that 20 % of the mass of the core had been dissolved during a 1.5 years long experiment. The core experienced axial shortening of 18 % (in length) and a porosity reduction of 20%.

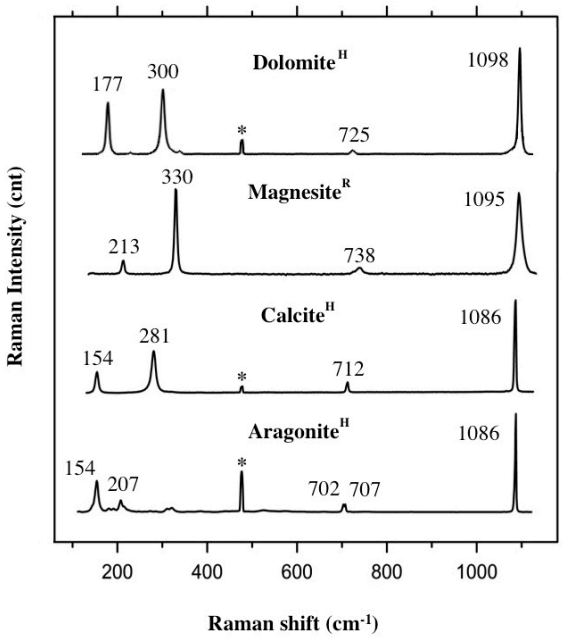

Figure 2. Raman spectra of calcium and magnesium carbonates: dolomite (UNIMIB standard sample, Selvino, Italy); magnesite (M.A.C. certificated standard); calcite (UNIMIB standard sample, Chihuahua, Mexico, ~ 0 mol% MgCO3), aragonite (UNIMIB – University of Milano Bicocca – standard sample, Val Formazza, Italy). Spectra with 'R' were analysed by the Renishaw inVia confocal Raman microscope and spectra with 'H' by Horiba Xplora. Stars represent the neon lamp emission line at 476.8 cm^{-1} used for calibration with the Horiba XploRA spectrometer. Peak positions are reported without decimals. After Borromeo et al. 2017a [49].

In the Long Term Test (LTT), using x-ray diffraction (XRD) [36], could detect the presence of magnesite, chrysotile (slice 1-3), tilleiyte (only in slice 4), quartz, anthophyllite as well as gypsum (the latter only in the unflooded chalk). Following a geochemical model [14], talc should precipitate, but this mineral could not be detected by XRD or other mineralogical analyses. Furthermore, magnesite could only be detected when it was rather abundant, and showed the limits of XRD as a detection method for traces of minerals. NanoSIMS 50 was the only analytical method that could detect positively with an image proof magnesite and very tiny new grown quartz of micron- and sub-micron sizes [36]. When analysed by MLA, the shorter of the two tests, LTT, displayed a rather sharp (~1.5 mm) transition between two areas with different mineralogy [59]. Closest to the inlet of the core, the rock material is completely altered into magnesite with minor contents of calcium along with clay minerals. In the area furthest away from the inlet, the mineralogy is still dominated by calcite, with occurrences of magnesite and clay, indicating only partial dissolution of calcite and precipitation of magnesite opposed to the complete substitution at the inlet. In the ULTT, the whole core showed similar composition, magnesite with the mentioned calcium impurities and clay.

Nermoen et al. (2015) [43] describes the flooding experiment of the 3-years-test (ULTT) in detail and a porosity decrease from 41.32 % to 40.02 % was observed at the end of the experiment, documenting how dissolution and precipitation of the solid volume may significantly alter the porosity evolution during compaction. The solid density increased from 2.68 to 2.90 g/cm^3 throughout the experiment, simultaneously the core has lost 22.93 g, which exemplifies that solid volume changes occur during flooding of $MgCl_2$ brines.

Common for the two tests is that compaction alone cannot explain the changes in permeability and porosity over time. For the ULTT [43] the permeability and calculated porosity are lowered during the start of the experiment where compaction is the controlling mechanism, while throughout the experiment, the permeability and porosity starts to increase again. This is believed to be caused by processes that involve mineralogical transformation through dissolution of primary and precipitation of secondary minerals. These changes in mineralogy is therefore an important factor to

both qualify and quantify to understand geomechanical alteration, as also seen in Wang et al. (2016) [37].

3. Results

3.1. FEG-SEM-EDS

The composition of the two cores after flooding has been affected by the nature of the fluid flow paths. This is often only visible at microscale, has a specific geometric form and is composed of several compositional trends [59] and therefore awaits a detailed study and is not of relevance here. Hence, a quick and thorough investigation of the mineralogical composition prior to detailed FEG-SEM-EDS studies or further meticulous electron- and ion-beam-based analyses would be helpful.

When studied by FEG-SEM-EDS, both the texture and the chemical composition of the chalk is significantly altered compared to the unflooded material (Fig. 3). The newly precipitated crystals are found in massive parts of the core (inlet part), with a homogenous high-magnesium carbonate composition as well as single crystals within the calcite dominated areas. The grains are no longer rounded, but show a rhombic crystal shape, with grain-size mostly below 1 µm. In the completely altered areas, coccoliths and other micro/nano-fossils are no longer observed, while in parts where the calcite is still present, clear signs of dissolution is visible [36, 59]. Additionally, significant amounts of clay-minerals are present, with main constituents being Mg and Si, which could be interpreted to be talc.

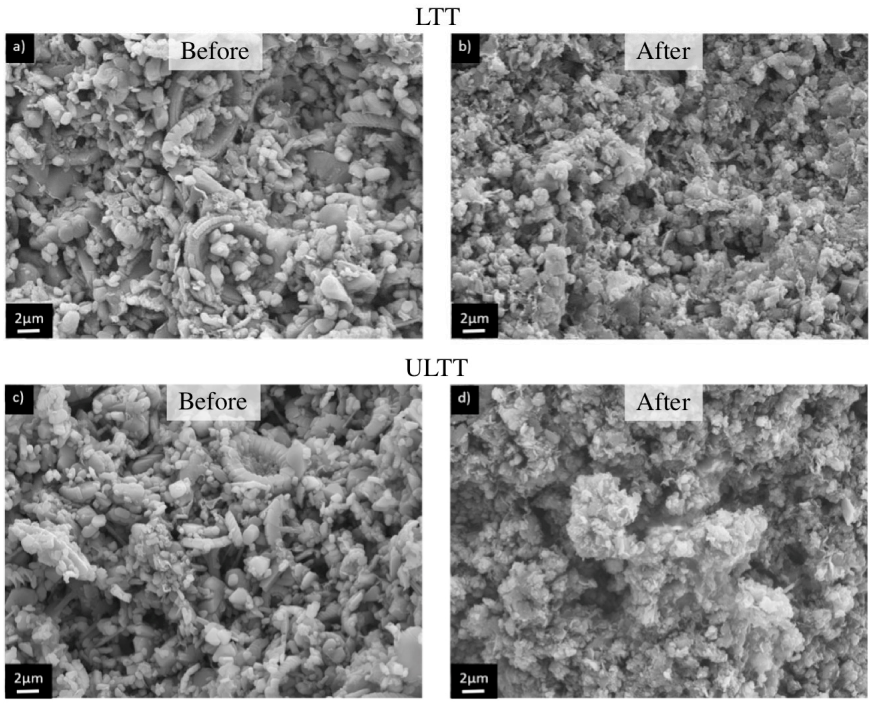

Figure 3. (**a**) SEM-micrograph of unflooded chalk from the end-piece of the LTT-core (from Zimmermann et al. 2015; [36]). Main components are coccoliths and fragments with a calcitic composition. (**b**) SEM-micrograph of the severely altered part of the flooded core (LTT) towards the inlet of the core (from Zimmermann et al. 2015 [36]). Coccoliths and other fossils are no longer visible, only crystals mainly below 1 µm in size, with high magnesium content. (**c**) SEM-micrograph of unflooded chalk of the ULTT with main components as observed in (a). (**d**) SEM-micrograph from slice 5 of the ULTT after flooding with $MgCl_2$. Texture and composition is as observed in (b).

3.2. Raman Spectroscopy

3.2.1. Generals

Peer-reviewed version available at Minerals 2018, 8, 221; doi:10.3390/min8060221

Raman spectroscopy has proven to be easy to use, but it requires an experienced operator to decide the setting of the instrument and how to interpret the spectra (see below). The mineralogical changes due to fluid injection were quickly evaluated: in few tens of seconds it was possible to distinguish the carbonate minerals present in the chalk (see Table 1). 647 spectra were collected, of which only 5 could not be identified, as they were not present in databases or literature. In LTT core 557 low region spectra were collected, 226 in slice 1 (120 in fragment 1, LT1_p1; 106 in fragment 2, LT1_p2), 220 in slice 2 (LT2), and 111 in slice 4 (LT4). In ULTT 90 spectra were collected in 9 different areas of the core.

In both ULTT and LTT cores no dolomite, aragonite, huntite, or high magnesium-calcite (45, 49) could be detected. As calcite Raman peaks positions reflect the magnesium content present in its lattice [49], it is possible to determine that the calcites present in ULTT and LTT always contain a low magnesium content (0 – 10 mol % ≈ 4 w.%; [49]) in the mineral.

Table 1. Mineral composition of the two cores: amounts and percentages of Raman spectra collected for each mineral in the Long Term Test (LTT) and in the Ultra Long Term Test (ULTT). When a two minerals spectrum was found, both components were counted to obtain the calcite/magnesite percentages.

	CALCITE		MAGNESITE		UNKNOWN		OTHER	
	spectra	%	spectra	%	spectra	%	spectra	%
LT1_p1A	20	77%	6	23%				
LT1_p1B	3	13%	20	87%				
LT1_p1C	20	87%	3	13%				
LT1_p1D	10	31%	20	63%	2	6%		
LT1_p1E	7	26%	20	74%				
LT1_p1F	18	60%	12	40%				
LT1_p1G	0	0%	22	96%			1 Brookite	4%
LT1_p1H	0	0%	25	100%				
LT1_p1I	0	0%	25	100%				
LT1_p2A	18	82%	4	18%				
LT1_p2B	2	10%	18	90%				
LT1_p2C	13	39%	20	61%				
LT1_p2D	16	53%	14	47%				
LT1_p2E	4	82%	16	18%				
LT2_A	71	92%	6	8%				
LT2_B	49	86%	7	12%	1	2%		
LT2_C	48	61%	31	39%				
LT2_D	30	41%	43	58%			1 Rutile	1%
LT4_A	19	79%	5	21%				
LT4_B	18	69%	6	23%	2	8%		
LT4_C	20	100%	0	0%				
LT4_D	20	100%	0	0%				
ULT1_1	3	23%	10	77%				
ULT2_4	1	9%	10	91%				
ULT2_5	0	0%	10	100%				
ULT2_5B	3	23%	10	77%				
ULT2_6	1	9%	10	91%				
ULT2_7	2	17%	10	83%				
ULT2_8	1	9%	10	91%				
ULT1_9	0	0%	9	100%				
ULT1_10	3	8%	10	92%				

Peer-reviewed version available at Minerals 2018, 8, 221; doi:10.3390/min8060221

An important issue regarding the results presented in this study (Table 1) that are shown as a percentage mineral/total is that we need to consider these % not as weight % or volume %, as the data express the presence of the signal of a mineral compared to the total of the collected spectra. When vibrational modes of both calcite and magnesite were detected simultaneously in one spectrum, both minerals were counted. In fact, occasionally, peaks of both calcite and magnesite were present in the same spectrum: this can happen when the analyses are performed on overlapped or very closely spaced fine grains (dimension of 1-2 µm), when the laser beams both grains at the same time and the laser diameter is too large. In this case, the detector collects photons scattered from the two minerals, resulting in a spectrum that is the mathematical sum of the two spectra of the two minerals (see Fig. 4). Consequently, the strong and sharp ν_1 peak (*symmetric stretching mode* of the carbonate ion) of both calcite and magnesite is present in one spectrum, respectively around 1086 and around 1095 cm^{-1} (25, 45, 46, 49) depending on the intensity, sharpness, and nearness of these two peaks, shoulders (asymmetric peaks) or double peaks (peaks with two edges) can be present (examples in Fig. 4). However, of importance is the fact that this can be detected. Another clear result of the simultaneous presence of calcite and magnesite signals in the same spectrum is given by the occurrence of the L (*librational mode)* peaks of the two carbonates at 280 and 330 cm^{-1} respectively. When a two minerals spectrum was found, both components were counted to obtain the calcite/magnesite percentages for each slice (see Table 1). It is important to point out that, as Raman spectroscopy can differentiate between the carbonate species, the spectrum collected in cases as the one described above (a magnesite and a calcite beamed at the same time, resulting in a combined spectrum) would be different from high Mg-calcite [49] or a dolomite spectrum (compare spectra shown in Fig. 2 and the ones presented in Fig. 4).

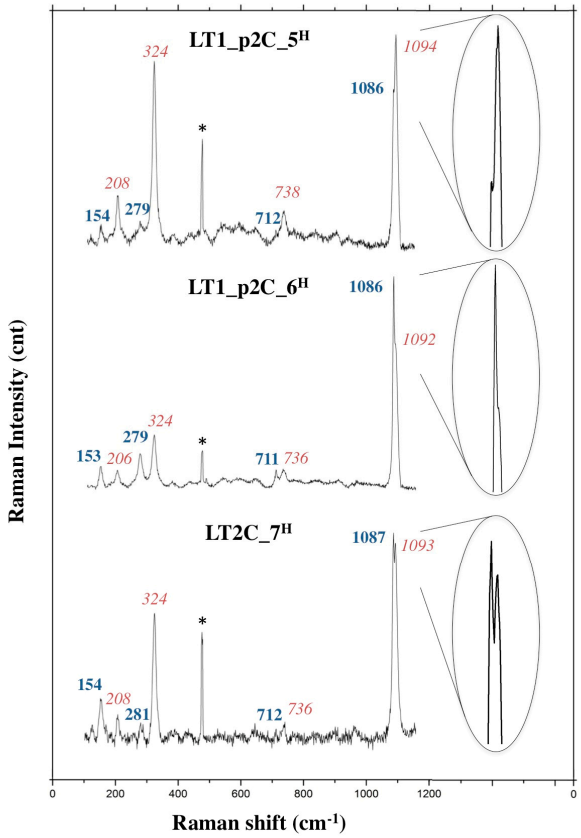

Figure 4. Raman spectra showing magnesite and calcite peaks in the same spectrum. This will happen when grains of 1-2 µm in size and different mineralogy are overlapped or placed very close: the laser beams both grains at the same time and as a consequence, the instrumentation detects the vibrational modes of both minerals. In LT1_p2C_5 the signal from magnesite is stronger than the calcite one, in LT1_p2C_6 it is weaker. The main peaks (ν^1, *symmetric stretching mode* of the carbonate ion) of the two

minerals are very close, generating a high peak with a "shoulder". In the third example shown, LT2C_7, the ν_1 of the two grains is so sharp and strong that a double peak is present. Calcite peaks are reported in blue/ bold, magnesite peaks in red/italic. All the spectra were collected with the Horiba XploRA spectrometer, stars represent the neon lamp emission line at 476. 8 cm^{-1} used for calibration. Peak positions are reported without decimals.

In order to detect the occurrence of hydrated silicates, the presence of diagnostic vibrational modes in the high frequencies region (2900-4200 cm^{-1}) of the Raman spectra was used, where the $(OH)^-$ vibrational modes are located [25, 64, 65]. The signal of phyllosilicates is quite weak and, in the 0-1200 cm^{-1} region, it is easily covered by the calcite and magnesite stronger intensity. As these two carbonates are anhydrous, they do not show peaks in the high region of the spectra. More than 200 high region spectra were collected in slice one, LT1_p2_B where an intense recrystallization of magnesite was already registered by Raman spectroscopy. The platy and very thin habit of phyllosilicates and clay minerals makes them really challenging to be detected, as it is very difficult to focus the laser inside their crystals and distinguish their weak scattering. Also, camera resolution and laser wavelength limit the analysis, and can lower the capability of focusing on the sample surface (under 1-2 µm in size).

3.2.2. Long Term Test

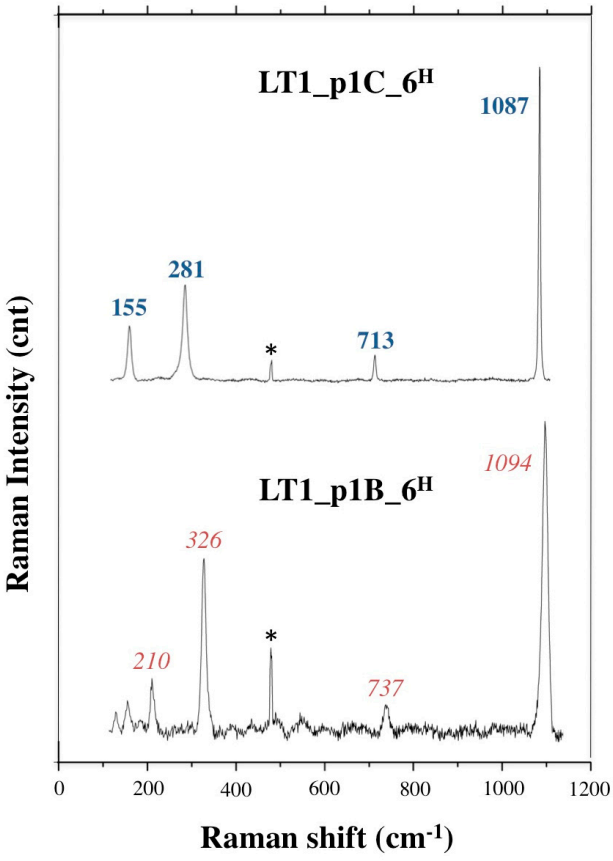

Figure 5. Raman spectra collected on the first slice of the Long Term Test. Raman showing the occurrence of the original calcite (LT1_p1C_6) and the presence of recrystallized magnesite (LT1_p1B_6). Calcite peaks are reported in blue/italic, magnesite peaks in red/bold. All the spectra were collected with the Horiba XploRA spectrometer, stars represent the neon lamp emission line at 476.8 cm^{-1} used for calibration with the Horiba XploRA spectrometer. Peak positions are reported without decimals.

Preprints (www.preprints.org) | NOT PEER-REVIEWED | Posted: 27 February 2018 doi:10.20944/preprints201802.0173.v1

Peer-reviewed version available at Minerals 2018, 8, 221; doi:10.3390/min8060221

Raman spectroscopy could identify the presence of recrystallized magnesite along the core of the Long Term Test up to 4 cm from the injection surface (see Figs. 5 and 6), which is also supported by Zimmermann et al. (2015) [36]. As predictable, the average alteration of the core is more pervasive close to the inlet surface, showing a decreasing amount of newly grown minerals with flooding direction (60 % of magnesite in slice 1-LT1; 30 % in in slice 2-LT2; and 10 % in slice 4-LT4; see Table 1 and Fig. 6). In Zimmermann et al. (2015) [36] positive XRD proof for magnesite could not be given in slice 4, but, however, geochemical data highlighted c. 3.9 % of MgO present in this slice, in comparison to 0.3 % of MgO in the unflooded material. In this study, only two non-carbonate crystals out of 647 Raman spectra were detected in LTT: brookite in LT1_p1_G and rutile in LT2_D (see Table 1 and Fig. 7).

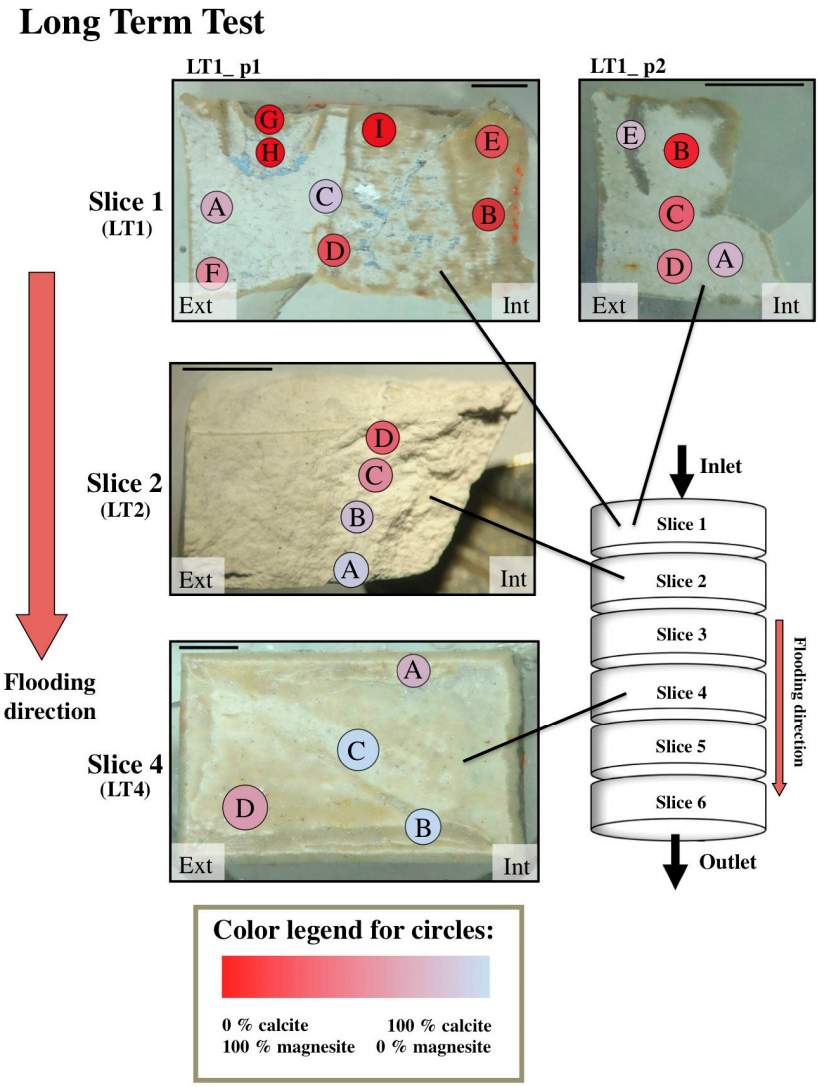

Figure 6. Mineralogical composition of the LTT core: 10 to 70 spectra have been collected in each of the area shown (9 areas in LT1_p1, 4 in LT1_p2, 4 in LT2, and 4 in LT4). Colour legend reflects the percentage of calcite and magnesite spectra collected in each area of the sample. See Table 1 for calcite and magnesite amounts and percentages obtained for each area. Flooding direction is indicated. Inner (core) end external (rim) parts of the samples are marked. The scales represent 0.25 cm. A schematic drawing (modified from Zimmermann et al. 2015 [36]) of how the cores were cut after the flooding experiment is shown to the right.

Two pieces of Slice 1 (LT1_p1 and LT1_p2, LTT; see Fig. 6) were analysed, with a total of 14 areas, and 226 Raman spectra (Table 1; Figs. 5 and 6).

In fragment 1 (LT1_p1) an intense magnesite regrowth is present in the inner portion of the core (LT1_p1 E and B 74, and 87 %, respectively, see Table 1 and Fig. 6), which becomes less pervasive close to the external rims (LT1_p1 A, F: 23, 40 %, respectively). In LT1_p1 a brown/ocre flow semi-circular structure is present and clearly visible to naked eye in the external part of the core; here a complete recrystallization to magnesite is present, reaching 100 % (LT1_p1 G and H, see Fig. 6). However, in this region, also a crystal of brookite (TiO_2) was detected (see Table 1 and Fig. 7). The average recrystallization of LT1_p2 is 47 %, and another textural element has been observed, a grey vein of calcite ($CaCO_3$ 82 %, LT1_p2 E, see Fig. 6). In order to try to detect hydrated minerals in LT1_p2, 210 high region spectra were collected. Unfortunately, no signal of clay minerals or talc was registered in any of them.

In Slice 2 (LT2; LTT) a longitudinal gradient in Mg content is perfectly detectable along flooding direction with a major magnesite recrystallization in the nearest areas to the inlet surface (from 58 (in LT2_D) to 8 (in LT2_A) %, see Table 1 and Fig. 6). Four areas were investigated in slice 2, with a total amount of 220 Raman spectra. A rutile spectrum was collected in LT2_D (see Table 1 and Fig. 7).

In Slice 4 (LT4; LTT) the recrystallization is less pervasive in the core than in the others (LT1 and LT2, LTT), as is the furthest from the inlet surface (Table 1; Fig. 6). A diagonal deep and pale grey structure crosses the LT4 slice (see Fig. 6) with a pure calcitic composition (111 spectra, 100 % of $CaCO_3$ no magnesite spectra were detected in this area). Some $MgCO_3$ spectra have been collected in a brownish area near the rim of the core (23 % of magnesite).

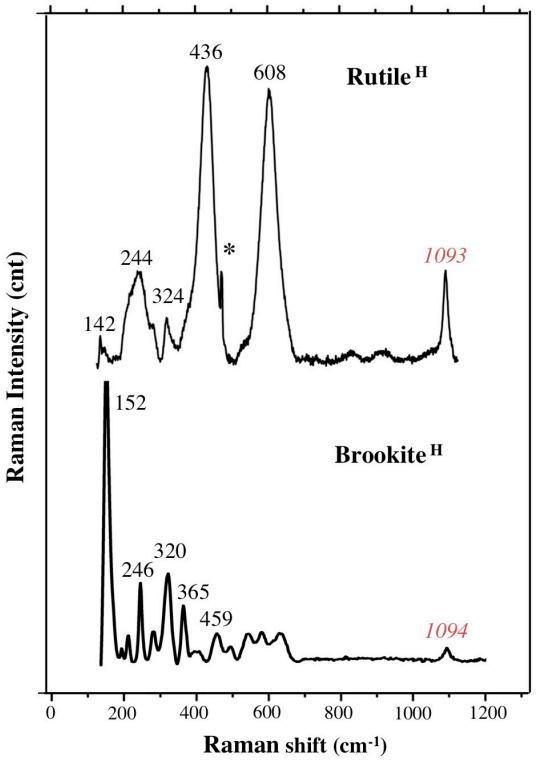

Figure 7. A brookite spectrum (identified in LT1_p1G) and one for rutile as identified in LT2_D (see Table 1). The main peak of magnesite (labelled in red) is present in both of them at 1093 and 1094 cm^{-1}, since the two minerals are surrounded by carbonates, which have a strong signal. Both spectra were collected whit the Horiba Xplora spectrometer, the star represents the neon lamp emission line at 476.8 cm^{-1} used for calibration. Peak positions are reported without decimals.

3.2.3. Ultra Long Term Test

The Ultra Long Term Test presents a widespread recrystallization of magnesite ($MgCO_3$) in the range of 77-100 % (see Table 1 and Figs. 8 and 9) along the entire core, and no alteration front was detectable anymore with Raman spectroscopy [43, 66].

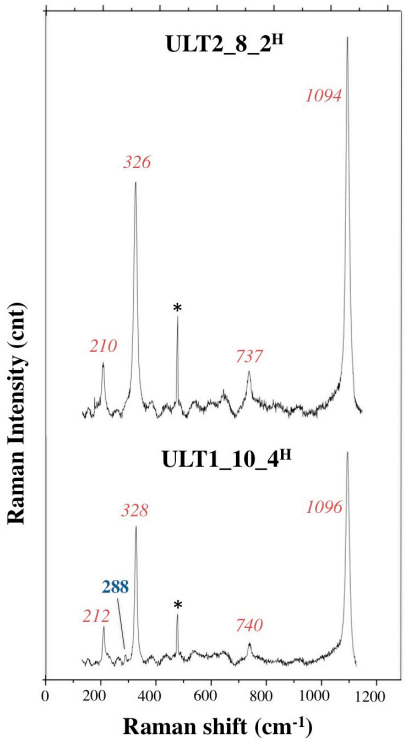

Figure 8. Raman spectra collected on the Ultra Long Term Test Raman showing the presence of recrystallized magnesite. The spectrum at the bottom of the figure (ULTT_10_4) shows the presence of a peak of calcite at 288 cm^{-1} (L, *librational mode*). Calcite peaks are reported in blue/bold, magnesite peaks in red/italic. Both spectra were collected with the Horiba XploRA spectrometer, stars represent the neon lamp emission line at 476.8 cm^{-1} used for calibration with the Horiba XploRA spectrometer. Peak positions are reported without decimals.

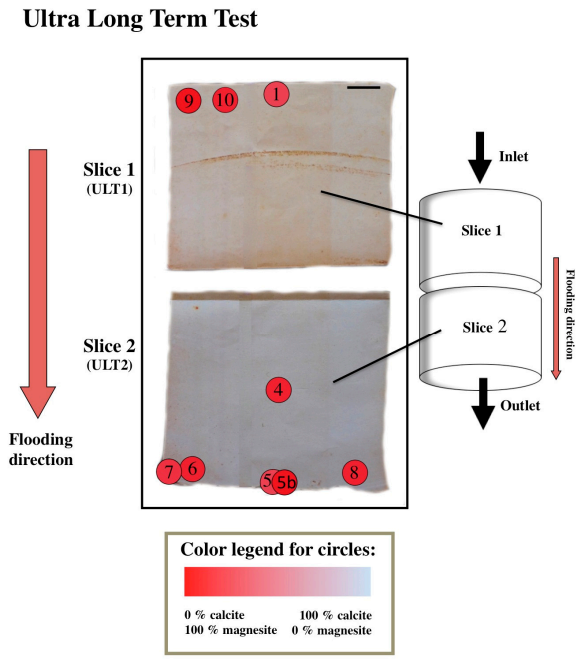

Figure 9. Mineralogical composition of the ULTT core: 10 spectra have been collected in each of the 9 areas shown. Colour legend reflects the percentage of calcite and magnesite spectra collected in each area of the sample. See Table 1 for calcite and magnesite amounts and percentages obtained for each area. Flooding direction is indicated. The scale represents 0.5 cm. A schematic drawing of how the cores were cut after the flooding experiment is shown to the right.

Raman spectra were collected in 9 different areas situated along the 7 cm core (90 spectra in total, see Table 1 and Fig. 9). No structures or patterns are visible to the naked eye and the core seems to be quite mineralogically homogeneous. Another study [60] made using ICP-MS (induced coupled plasma mass spectrometry) confirmed our data as average of 4 % of CaO was detected on the bulk sample, with no great difference in composition in the different portions of the sample.

4. Discussion

This study represents the first attempt to apply Raman spectroscopy to chalk mineralogy with a single grain approach on micron scale. The very fine-grained and soft texture of this sedimentary rock made detailed analysis quite challenging with common methods, and for this reason in the last years several high performing techniques have been included in Enhanced Oil Recovery (EOR) research. Raman spectroscopy, thanks to its quickness, low cost, and micrometric resolution, turned out to be very suitable for these studies as, in few seconds and without any sample preparation, a mineralogical identification can be provided. It is perfectly complementary to methods such as SEM-EDS.

The major alteration front in LTT was previously suggested between LT3 and LT4 [36], however by the use of Raman spectroscopy, it was possible to detect magnesite even in slice 4 (Table 1; Fig. 6), when XRD studies could not be positive in this regard [36]. The calcite dissolution and magnesite recrystallization were massive in the first 2 cm of the core (slice 1 and 2 of LTT; Fig. 6). LTT5 and LTT6 were not studied in this investigation as in a previous study [36], these slices were found to be the least altered slices by the flooding unable to provide further information when applying the used methods. Raman spectroscopy confirmed that such an alteration front was no longer present within the ULTT, which means that in three years of $MgCl_2$ injection, a sufficient quantity of Mg^{2+} was flooded into the core [43], permitting the substitution of almost all the Ca^{2+} to take place (92 % of magnesite Raman spectra; see Table 1 and Fig. 9).

As already seen with other techniques (SEM, XRD) applied in a previous study [36] it was not possible to identify clay-minerals in the two cores using Raman spectroscopy. It is very difficult to find a technique that could provide a resolution high enough to spot <1 μm crystals and simultaneously have the capability to cover a portion of the sample wide enough to detect a ≤ 5 % component, in a quick way, and image it at the same time. A principle technique would be a Mineral Liberation Analyser (MLA) with a nanometre-small spot size, which is still technically challenging using electron-beams on such small scales, or a Nano-scale Secondary Ion Mass Spectrometer (nano-SIMS) [36] or nanoRaman (TERS, Tip Enhanced Raman Spectroscopy) [61,62], application coupled with an Atomic Force Microscope (AFM). In the LTT sample nano-crystals of quartz has been detected only by nano-SIMS [36], which is a very time-consuming and destructive methodology, extraordinarily expensive and not quantitative. Another technique would be TEM-EDS (Transmission Electron Microscopy) with the same critique points besides that the latter reveals quantitative data along with mineral-identification through diffraction analysis [63]. Raman spectroscopy could be the tool to use but with the known limits of 1-2 micron spotsize and the impossibility to image the analysed area with an optical microscope. An advance would be to scan an area, which is still a technical issue. A very low abundance of a mineral may be challenging to detect unless collecting a really huge number of spectra, which in turn would be time consuming. Furthermore, the identification of small and thin hydrated minerals is quite difficult to achieve in the 0-1200 cm^{-1} region of the Raman spectra, since their signal is weak and easily covered by the higher carbonate peaks. For this reason, we tried to detect them with a different setting of the instrumentation, moving the analyses to the high region of the Raman spectra, around 3500 cm^{-1}, where the OH^- vibrational modes are present. Anhydrous minerals such as calcite and magnesite do not show peaks in this region. Unfortunately, no signal from phyllosilicates has been detected, possibly as a consequence of these technical difficulties.

Despite the impossibility to recognise so low-concentrated and platy minerals, since the set-up is relatively economical and rapid the authors think that Raman spectroscopy represents a very helpful methodology that could and should be used on hydrocarbon drilling rigs, possibly even as a

414 drilling steering tool, because carefully investigations could show that positive and useful results
415 were generated. This can lead to well-developed methodologies in the future for different
416 approaches, like the petroleum industry.

417 **5. Conclusions**

418 The mineralogical and textural changes that follow dissolution, precipitation and compaction in
419 brine-injected chalk affect the permeability, porosity, reservoir potential, and the oil flow pathways
420 (e.g. 8, 21, 36, 59). For this reason, a deep investigation of secondary mineral recrystallization is of
421 paramount importance in EOR research.
422 This study demonstrates that Raman spectroscopy is a robust, cheap, user-friendly point-
423 analysis technique that with a non-destructive sample preparation allows to quickly obtain semi-
424 quantitative mineralogical and chemical information. This method has been applied to micron-sized
425 chalk samples, giving an advantage in comparison to time consuming methods like SEM, thin section
426 studies, nano-Raman or EMPA, and ion-probe analysis. An estimation of the magnesite
427 recrystallization could be performed on two chalk cores that were flooded under reservoir conditions
428 with $MgCl_2$: Long Term Test (1.5-years-test, LTT) and Ultra Long Term Test (3-years-test, ULTT). In
429 the LTT the average recrystallization is more pervasive close to the inlet surface and varies with
430 flooding direction from c. 60 % (slice 1) to c. 10 % (slice 4). ULTT is, on the other hand, quite
431 homogeneous, as the alteration front is no longer visible and the whole core is predominantly
432 consisting of magnesite (92 %).
433 However, not all reservoir rocks do contain minerals and/or phases as small as those in chalk,
434 which would make the here shown methodology very attractive. Raman spectroscopy can, together
435 with other research methods, provide a full range of information on flooded chalk cores for a broader
436 understanding of chemical and mineralogical changes in those samples during the mentioned EOR
437 experiments.
438 Until today Raman spectroscopy has been only occasionally applied in the oil industry [67- 70]
439 and it is time for it to become a routine analysis.

440 **Acknowledgments:** The authors acknowledge the Research Council of Norway and the
441 industry partners; ConocoPhillips Skandinavia AS, Aker BP ASA, Eni Norge AS, Maersk Oil Norway AS, Statoil
442 Petroleum AS, ENGIE E&P NORGE AS, Lundin Norway AS, Halliburton AS, Schlumberger Norge AS,
443 Wintershall Norge AS, DEA Norge AS of The National IOR Centre of Norway for support.

444 This study is a central part of the PhD thesis of LB who thanks the NIOR Centre of Norway for a grant to carry
445 out the research, Eduardo Garzanti and the group of Provenance Studies (University of Milano – Bicocca) for
446 their advices.

447 **Author Contributions:** L.B. made a substantial contribution to every step of the study, such as acquisition (with
448 the fundamental help of N.E.) and interpretation of the data and writing of the paper. U.Z., L.B, MW.M. and S.A.
449 contributed to design and conception of the present publication. M.V.M. and R.I.K. designed and performed the
450 long-term tests on the chalk cores. All the co-authors performed a critical revision of the intellectual content of
451 the paper.

452 **Conflicts of Interest:** The authors declare no conflict of interest. The founding sponsors had no role in the design
453 of the study; in the collection, analyses, or interpretation of data; in the writing of the manuscript, and in the
454 decision to publish the results.

455 **References**

456 1. Hermansen, H; Landa, G. H.; Sylte, J. E.; Thomas, L. K. Experiences after 10 years of waterflooding the
457 Ekofisk Field, Norway. *J. Pet. Sci. Eng*. **2000**, *26.1*, 11-18.
458 2. Nagel, N. B. Compaction and subsidence issues within the petroleum industry: from Wilmington to Ekofisk
459 and beyond. *Phys. Chem. Earth A*. **2001**, *26*, 3-14.
460 3. Risnes, R.; Madland M. V.; Hole M.; Kwabiah N. K. Water weakening of chalk – Mechanical effects of water-
461 glycol mixtures, *J. Pet. Sci. Eng*. **2005**, *48*, 21-36.

4. Heggheim, T.; Madland, M. V.; Risnes, R.; Austad, T. A chemical induced enhanced weakening of chalk by seawater. *J. Pet. Sci. Eng*. **2005**, *46*(3), 171-184.
5. Korsnes, R. I.; Strand S.; Hoff Ø.; Pedersen T.; Madland M. V.; Austad T. Does the chemical interaction between seawater and chalk affect the mechanical properties of chalk? In *Multiphysics coupling and long term behaviour in rock mechanics*; Cotthem; A. V.; Charlier R.; Thimus J. F. and Tshibangu J. P. Eds.; Taylor & Francis: London, England, **2006**; pp. 427-434.
6. Korsnes, R. I.; Madland, M. V.; Austad, T.; Haver, S.; Rosland, G. The effects of temperature on the water weakening of chalk by seawater. *J. Pet. Sci. Eng*. **2008a**, *60*, 183- 193.
7. Madland, M. V.; Midtgarden, K.; Manafov, R.; Korsnes, R. I.; Kristiansen, T.; Hiorth, A. The Effect of Temperature and Brine Composition on the Mechanical Strength of Kansas Chalk. *International Symposium of the Society of Core Analysts,* Abu Dhabi, **2008**, 6.
8. Madland, M.V.; Hiorth, A.; Omdal E.; Megawati M.; Hildebrand-Habel T.; Korsnes I. R.; Evje S.; Cathles M. L. Chemical alterations induced by rock-fluid interactions when injecting brines in high porosity chalks, *Transp. Porous Med*. **2011**, *87*, 679-702.
9. Zangiabadi, B.; Korsnes, R. I.; Hildebrand-Habel, T.; Hiorth, A.; Surtarjana, I. K.; Lian, A.; Madland, M. V. Chemical water weakening of various outcrop chalks at elevated temperature. In *Poromechanics IV*, Ling H. I., Smyth A., and Betti, R., Eds. DEStech Publications, Inc., Lancaster, England, **2009**; pp. 543-548.
10. Andreassen, K.A. and Fabricius, I. L. Biot critical frequency applied to description of failure and yield of highly porous chalk with different pore fluids, *Geophysics*, **2010**, *75*(6), E205-E213.
11. Zhang, P.; Tweheyo, M.T.; Austad T.; Wettability alteration and improved oil recovery by spontaneous imbibition of seawater into chalk: impact of the potential determining ions Ca^{2+}, Mg^{2+}, and SO_4^{2+}, *Colloids Surf. A Physicochem. Eng. Aspects*, **2007**, *301*, 199–208.
12. Strand, S.; Hjuler, M. L.; Torsvik, R.; Pedersen, J. I.; Madland, M. V.; Austad, T. Wettability of chalk: impact of silica, clay content and mechanical properties. *Petroleum Geoscience*, **2007**, *13*(1), 69-80.
13. Austad, T.; Strand, S.; Madland, M.V.; Puntervold, T.; Korsnes, R.I. Seawater in chalk: An EOR and compaction fluid, *SPE Reservoir Evaluation and Engineering*, **2008**, *11*(4), 648-654.
14. Hiorth, A.; Cathles, L.; Madland, M. The Impact of Pore Water Chemistry on Carbonate Surface Charge and Oil Wettability, *Transp. Porous Med*. **2010**, *85*(1), 1–21.
15. Fathi, S.J.; Austad, T.; Strand, S. "Smart Water" as a Wettability Modifier in Chalk: The Effect of Salinity and Ionic Composition, *Energy & fuels*, **2010**, *24*, 2514-2519.
16. Ali, A.Y., Salah Hamad, A.S., Abdulaziz, A.K.; Mohammed Saleh, A.J., Laboratory Investigation of the Impact of Injection Water Salinity and Ionic Content on Oil Recovery From Carbonate Reservoirs, *SPE Reservoir Evaluation & Engineering*, **2011**.
17. Megawati, M.; Hiorth, A.; Madland, M. V. The impact of surface charge on the mechanical behavior of high-porosity chalk. *Rock Mech. Rock Eng*. **2013**, *46.5*, 1073-1090.
18. Zhang, P.; Tweheyo, M. T.; Austad, T. Wettability Alteration and Improved Oil Recovery in Chalk: The Effect of Calcium in the Presence of Sulfate. Energy & Fuels, **2006**, 20(5), 2056-2062.
19. Andersen, P.Ø., Evje, S., Madland, M.V.; Hiorth, A., A geochemical model for interpretation of chalk core flooding experiments, *Chem. Eng. Sci.* **2012**, *84*, 218-241.
20. Megawati, M.; Madland, M. V.; Hiorth, A. Mechanical and physical behavior of high-porosity chalks exposed to chemical perturbation: *J. Pet. Sci. Eng*. **2015**, *133*, 313-327.
21. Wang, W.; Madland, M. V.; Zimmermann, U.; Nermoen, A.; Reidar, I.; Korsnes, R.; Bertolino, S. R. A.; Hildebrand-Habel, T. Evaluation of porosity change during chemo-mechanical compaction in flooding experiments on Liege outcrop chalk. In *Reservoir Quality of Clastic and Carbonate Rocks: Analysis, Modelling and Prediction*. Armitage, P. J.; Butcher, A. R.; Churchill, J. M.; Csoma, A. E.; Hollis, C.; Lander, R. H.; Omma, J. E. & Worden, R. H. Eds.; Geological Society: London, England, **2016**, Special Publications, 435.
22. Raman, C.V. A new radiation. *Indian J. Phys*. **1928**, *2*, 387–398.
23. Krishnamurti, D. Raman spectrum of magnesite. *Proceedings of the Indian Academy of Sciences – Section A* **1956**, 43, 210.
24. Griffith, W.P., Raman spectroscopy of minerals. *Nature* **1969**, *224*, 264–266.
25. Kuebler, K.; Wang A.; Abbott, K.; Haskin, L. A. Can we detect carbonate and sulfate minerals on the surface of Mars by Raman spectroscopy? *Lunar and Planetary Science XXXII* **2001**, n. 1889.

26. Downs, R. T. "The RRUFF Project: an integrated study of the chemistry, crystallography, Raman and infrared spectroscopy of minerals." In *Program and Abstracts of the 19th General Meeting of the International Mineralogical Association in Kobe, Japan, 2006*. **2006**.
27. Andò, S. and Garzanti, E. Raman spectroscopy in heavy-mineral studies. In *Sediment Provenance Studies in Hydrocarbon Exploration and Production* Scott, R. A., Smyth, H. R., Morton, A. C. & Richardson, N. Eds. Geological Society: London, England, Special Publications, 2013, 386.
28. Gillet, P.; Biellmann, C.; Reynard, B.; McMillan, P. Raman spectroscopic studies of carbonates Part I: High-pressure and high-temperature behaviour of calcite, magnesite, dolomite and aragonite. *Phys. Chem. Minerals*, **1993**; *20* (1), 1-18.
29. Bendel, V. and Schmidt, B. C. Raman spectroscopic characterisation of disordered alkali feldspars along the join $KAlSi_3O_8$–$NaAlSi_3O_8$: application to natural sanidine and anorthoclase. *Eur. J. Mineral.* **2008**, *20*, 1055–1065.
30. Noguchi, N.; Abduriyim, A.; Shimizu, I.; Kamegata, N.; Odake, S.; Kagi, H. Imaging of internal stress around a mineral inclusion in a sapphire crystal: application of micro-Raman and photoluminescence spectroscopy. *JRS.* **2013**, *44*(1), 147-154.
31. De La Pierre, M.; Carteret, C.; Maschio, L.; André, E.; Orlando, R.; Dovesi, R. The Raman spectrum of $CaCO_3$ polymorphs calcite and aragonite: a combined experimental and computational study. *J. Chem. Phys.* **2014**, *140(16)*, 164509.
32. Del Monte, B.; Paleari, C. I.; Andò, S.; Garzanti, E.; Andersson, P. S.; Petit, J. R.; Crosta, X.; Narcisi, B.; Baroni, C.; Salvatore, M. C.; Baccolo, G.; Maggi V. Causes of dust size variability in central East Antarctica (Dome B): Atmospheric transport from expanded South American sources during Marine Isotope Stage 2. *Quat. Sci. Rev.* **2017**, *168*, 55-68.
33. Molenaar, N. and Zijlstra, J. J. P. Differential early diagenetic low-Mg calcite cementation and rhythmic hardground development in Campanian-Maastrichtian chalk. *Sediment. Geol.*, **1997**, *109*(3-4), 261-281.
34. Robaszynski, F.; Dhondt, A. V.; John, W. M. Cretaceous lithostratigraphic units (Belgium). *Geol. Belg.* **2001**, *4 1-2*, 121-134.
35. Hjuler, M.L.; Fabricius, I.L. Engineering properties of chalk related to diagenetic variations of Upper Cretaceous onshore and offshore chalk in the North Sea area. *J. Pet. Sci. Eng*. **2009**, *68*, 151–170. DOI: 10.1016/j.petrol.2009.06.005.
36. Zimmermann, U.; Madland, M. V.; Nermoen, A.; Hildebrand-Habel, T.; Bertolino, S. A. R.; Hiorth, A.; Korsnes, R. I.; Audinot, J. N.; Grysan P. Evaluation of the compositional changes during flooding of reactive fluids using scanning electron microscopy, nano-secondary ion mass spectroscopy, x-ray diffraction, and whole-rock geochemistry: *AAPG. Bulletin*, **2015**, *99*, 791-805.
37. Wang, W., Madland, M.V., Zimmermann, U., Nermoen, A., Korsnes, R.I., Bertolino, S.R.A., Hildebrand-Habel, T. Evaluation of porosity change during chemo-mechanical compaction in flooding experiments on Liège outcrop chalk. *Geol. Soc. Spec. Publ.* **2016**; DOI: 10.1144/SP435.10
38. Hjuler, M. L., and Fabricius, I. L. Diagenesis of upper cretaceous onshore and offshore chalk from the North Sea area. Technical University of Denmark, Department of Civil Engineering, Arctic Technology Centre, ARTEK, **2007**.
39. Felder, R. M.; Spence, R. D.; Ferrell, J. K. A method for the dynamic measurement of diffusivities of gases in polymers. *J. Polym. Sci.* **1975**. *19(12)*, 3193-3200.
40. Molenaar, N., and Zijlstra, J. J. P. Differential early diagenetic low-Mg calcite cementation and rhythmic hardground development in Campanian-Maastrichtian chalk. *Sediment. Geol.* **1997**, *109*(3-4), 261-281.
41. Slimani, H. New species of dinoflagellate cysts from the Campanian-Danian chalks at Hallembaye and Turnhout (Belgium) and at Beutenaken (the Netherlands), *J. Micropalaeontol.* **2001**, *20* (1), p. 1–11, DOI:10.1144/jm .20.1.1.
42. Strand, S.; Hjuler, M. L.; Torsvik, R.; Pedersen, J. I.; Madland, M. V.; Austad, T. Wettability of chalk: impact of silica, clay content and mechanical properties. *Petrol. Geosc.* **2007**, *13*(1), 69-80.
43. Nermoen, A.; Korsnes, R. I.; Hiorth, A.; Madland, M. V. Porosity and permeability development in compacting chalks during flooding of nonequilibrium brines: Insights from long-term experiment. *JGR: Solid Earth* **2015**, *120*(5), 2935-2960.
44. Rutt, H. N. and Nicola, H. J. Raman spectra of carbonates of calcite structure. *Phys. C: Solid State Phys.* **1974**, *7*, *4522.*

45. Bischoff, W. D.; Sharma, S. K.; MacKenzie, F. T. Carbonate ion disorder in synthetic and biogenic magnesian calcites: a Raman spectral study. *Am. Mineral.* **1985**, *70*(5-6), 581-589.
46. Herman, R. G.; Bogdan, C. E.; Sommer, A. J.; Simpson, D. R. Discrimination among carbonate minerals by Raman spectroscopy using the laser microprobe. *Appl. Spectrosc.***1987**, *41*(3), 437-440.
47. Edwards, H.; Villar, S.; Jehlicka, J.; Munshi, T. FT–Raman spectroscopic study of calcium-rich and magnesium-rich carbonate minerals. *Spectrochim. Acta A*, **2005**; *61*, 2273.
48. Korsakov, A.; De Gussem, K.; Zhukov, V. P.; Perraki, M.; Vandenabeele, P.; Golovin, A. V. Aragonite-calcite-dolomite relationships in UHPM polycrystalline carbonate inclusions from the Kokchetav Massif, northern Kazakhstan. *Eur. J. Mineral.* **2009**, *21*, 1301.
49. Borromeo, L.; Zimmermann, U.; Andò, S.; Coletti, G.; Bersani, D.; Basso, D.; Gentile, P.; Schulz, B. and Garzanti, E. Raman spectroscopy as a tool for magnesium estimation in Mg-calcite. *JRS.* **2017a**, *48*(7), 983-992.
50. Dandeu, A.; Humbert, B.; Carteret, C.; Muhr, H.; Plasari, E.; Bossoutrot, J. M. Raman Spectroscopy – A Powerful Tool for the Quantitative Determination of the Composition of Polymorph Mixtures: Application to CaCO3 Polymorph Mixtures. *Chem. Eng. Technol*. **2006**; *29*, 221.
51. Carteret, C.; De La Pierre, M.; Dossot, M.; Pascale, F.; Erba, A.; Dovesi, R. The vibrational spectrum of CaCO3 aragonite: A combined experimental and quantum-mechanical investigation. *J. Chem. Phys.* **2013**; *138*, 014201.
52. Sun, J.; Zeguang, W.; Hongfei, C. A Raman spectroscopic comparison of calcite and dolomite, *Spectrochim. Acta A*, **2014**; *117*, 158.
53. Purgstaller, B.; Mavromatis, V.; Immenhauser, A.; Dietzel, M. Transformation of Mg-bearing amorphous calcium carbonate to Mg-calcite – In situ monitoring. *Geoch. Et Cosmoch. Acta,* **2016**, *174*, 180–195.
54. Krishnan, R. S. Proc. Math. Sci. **1945**; Part. I: Calcite, 182.
55. White, W.B., In *Infrared Spectra of Minerals,* V.C. Farmer Eds. Mineralogical Society Monograph 4, Mineralogical Society, London, England, **1974a**, pp 87–110.
56. White, W.B., In *Infrared Spectra of Minerals,* V.C. Farmer Eds. Mineralogical Society Monograph 4, Mineralogical Society, London, England, **1974b**, pp 227– 284.
57. Gillet, P.; Biellmann, C.; Reynard, B.; McMillan, P. Raman spectroscopic studies of carbonates Part I: High-pressure and high-temperature behaviour of calcite, magnesite, dolomite and aragonite. *Phys. Chem. Minerals* **1993**; *20* (1), 1-18.
58. Urmos, J.; Sharma, S. K.; Mackenzie, T. Characterization of some biogenic carbonates with Raman spectroscopy, *Am. Mineral.* **1991**; *76*, 641.
59. Minde, M. W.; Haser, S.; Korsnes, R. I.; Zimmermann, U.; Madland, M. V. Comparative Studies of Mineralogical Alterations of Three Ultra-long-term Tests of Onshore Chalk at Reservoir Conditions. In *IOR 2017-19th European Symposium on Improved Oil Recovery 2017*, **2017**.
60. Minde, M. W.; Zimmermann, U.; Madland, M. V., Korsnes, R. I. Submicron investigations –What can we learn? IOR Norway 2016, Stavanger, **2016**.
61. Borromeo, L.; Minde, M.; Toccafondi, C.; Zimmermann, U.; Andò, S.; Ossikovski R. A New Frontier Technique for Nano-analysis on Flooded Chalk-TERS (Tip Enhanced Raman Spectroscopy). In *IOR 2017-19th European Symposium on Improved Oil Recovery*. **2017b**.
62. Borromeo, L.; Toccafondi, C.; Minde, M.; Zimmermann, U.; Andò, S.; Madland, M. V., Korsnes, R. I. Ossikovski R. Application of Tip Enhanced Raman Spectroscopy in the nanoscale characterization of flooded chalk. Submitted to Minerals, January **2018**;
63. Egeland, N.; Minde, M.W.; Kobayashi, K.; Ota, T.; Nakamura, E.; Zimmermann, U.; Madland, M.W. and Korsnes, R.I.. Quantification of Mineralogical Changes in Flooded Carbonate under Reservoir Conditions. In *IOR 2017-19th European Symposium on Improved Oil Recovery*. **2017**.
64. Frezzotti, M. L.; Tecce, F.; Casagli. A. Raman spectroscopy for fluid inclusion analysis, *J Geochem Explor.* **2012**, 112, 1–20;
65. Wang, A.; Freeman, J. J.; Jolliff, B. L. Understanding the Raman spectral features of phyllosilicates, *JRS*, **2015**, *46*, 829–845.
66. Egeland, N. Raman Spectroscopy Applied to Enhanced Oil Recovery. University of Stavanger, unpublished MSc thesis, **2015**.
67. Gorelik, V. S.; Chervyakov, A. V.; Kol'tsova, L. V.; Veryaskin, S. S. Raman Spectra of Saturated Hydrocarbons and Gasolines. *J. Russ. Laser Res.* **2000**, *21*, 323-334.

621 68. Costa, J. C. S.; Sant'Ana, A. C.; Corio P; Temperini, M. L. A. Chemical analysis of polycyclic aromatic
622 hydrocarbons by surface-enhanced Raman spectroscopy. *Talanta* **2006**, *70*, 1011-1016.
623 69. Sebek, J.; Pele, L.; Potma, E. O.; Gerber, R. B. Raman spectra of long chain hydrocarbons: anharmonic
624 calculations, experiment and implications for imaging of biomembranes. *PCCP*, **2011**, *13*, 12724-12733.
625 70. Andrews, A. B.; Wang D.; Marzec, K. M.; Mullins, O. C.; Crozier, K. B. Surface enhanced Raman
626 spectroscopy of polycyclic aromatic hydrocarbons and molecular asphaltenes. *Chem. Phys. Lett.* **2015**, *620*,
627 139-143.